Influence of Ti and Cu on the Corrosion Properties of Laser-Deposited High Entropy Alloys

1st Modupeola Dada
Department of Chemical, Metallurgical and Materials Engineering, Tshwane University of Technology, Staatsartillerie Rd, Pretoria West,
Pretoria, South Africa
dadadupeola@gmail.com

2nd Patricia Popoola
Department of Chemical, Metallurgical and Materials Engineering, Tshwane University of Technology, Staatsartillerie Rd, Pretoria West,
Pretoria, South Africa
popoolaAPI@tut.ac.za

3rd Ntombi Mathe
National Laser Centre, Council for Scientific and Industrial Research, Meiring Naudé Road, Brummeria,
Pretoria, South Africa
NMathe@csir.co.za

4th Sisa Pityana
National Laser Centre Council for Scientific and Industrial Research, Meiring Naudé Road, Brummeria,
Pretoria, South Africa
Spityana@csir.co.za

5th Samson Adeosun
Department of Metallurgical and Materials Engineering line 3: *name of organization*
University of Lagos
Lagos, Nigeria
sadeosun@unilag.edu.ng

6th Thembisile Dlamini
National Laser Centre Council for Scientific and Industrial Research, Meiring Naudé Road, Brummeria,
Pretoria, South Africa
TDlamini2@csir.co.za

7th Olufemi Aramide
Department of Chemical, Metallurgical and Materials Engineering, Tshwane University of Technology, Staatsartillerie Rd, Pretoria West,
Pretoria, South Africa
foaramide@tut.ac.za

***Abstract*— In this study, AlCoCrFeNiCu (Cu-based) and AlCoCrFeNiTi (Ti-based) high entropy alloys were fabricated using laser additive manufacturing. The influence of the alloying elements and the laser processing parameters, the laser power and scanning speed on the corrosion behaviour of high entropy alloys for improved corrosion resistance were examined. The corrosion resistance in 1 mol/L sodium hydroxide solution was investigated using potentiodynamic polarization in experimental conditions at ambient temperature. Results indicate that the scan speed and laser power are two interactive factors that influence the corrosion rates, however, the laser power had more influence. Optimization occurred at 1400 W laser power and a scan speed of 10 mm/s. The Cu-based alloy with a corrosion rate of 0.00197 mm/yr was more resistant to corrosion than the Ti-based alloy with corrosion rates of 0.002635 mm/yr under optimum conditions.**

Keywords— Corrosion rate, High Entropy Alloys, Laser Additive Manufacturing, Sodium Hydroxide, Response Surface Methodology

I. Introduction

High entropy alloys (HEAs) are a new class of alloy system that supersedes the traditional strategy of alloy development where one or two principal elements are selected with other minor elements for modification purposes. According to Yeh et al. [1], HEAs have five or more principal element with an atomic percentage ranging between 5 and 35. These amalgams in literature have been reported to show excellent mechanical and high-temperature properties attributed to their characteristic feature of forming solid solutions at elevated temperatures. This attribute makes HEAs suitable for several applications which require thermal stability and strength. Zhang et al. [2] reported that HEAs are promising materials for aerospace applications. Zhu et al. [3] stated that the AlCoCrFeNi high entropy alloy (HEA) is one of the most studied compositions, which acts as an excellent binder attributed to its high entropy mixing effect. This alloying system has a wide range of other properties with the inclusion of other alloying elements. Ma et al. [4] investigated the influence of adding Nb to the HEA composition, and the authors mentioned the alloy's microhardness and yield strength increased linearly with an increase in Nb content. Dong et al. [5] studied the influence of vanadium in the AlCoCrFeNi HEA composition; the authors recorded an increase in the plastic strain, microhardness and compressive strength of the alloy with an increase in the vanadium content. Chen et al. [6] reported that the minor addition of Zr to the AlCoCrFeNi HEA composition significantly increased the mechanical properties of the alloy. Most reports in literature were on the influence of these elements on the mechanical property of AlCoCrFeNi HEA; however, the reports on the corrosion resistance of AlCoCrFeNiCu and AlCoCrFeNiTi HEAs fabricated by laser additive manufacturing in 1 mol/L NaOH solution are limited. To get the best results from the corrosion experiments of laser HEAs, there is a need to first optimize the process parameters. According to Nemati-Chari et al. [7], conventional optimization methods like SPSS, Statistica and Minitab; do not consider all parameters at the same time; only one parameter at a time is measured while others are kept constant thus, making the optimization process time consuming and expensive. Response surface methodology (RSM) is an alternative method of optimization which evaluates various laser processing parameters and their desired responses in several runs or experiments [8]. Vakili-Azghandi et al. [9] used RSM to develop regressive models to predict the corrosion behaviour of an alloy coating. Barcelos et al. [10] applied RSM in evaluating the elemental content and weight loss of Ni-Ti commercial orthodontic wires and stainless steel in an artificial saliva solution. Goh et al. [11] used RSM to optimize the operating conditions, which use an inhibitor in reducing copper corrosion. Rashid et al. [12] used RSM to optimize parameters for the corrosion rate of carbon steel in saline water. Saeidi et al. [13] explored RSM in optimizing the pressure and temperature parameters of carbon dioxide in a sodium hydroxide solution. In this study, AlCoCrFeNiCu (Cu-based) and AlCoCrFeNiTi (Ti-based) HEAs were fabricated using laser additive manufacturing (LAM) and potentiodynamic polarization was used to analyze the corrosion responses of the alloys in 1 mol/L NaOH solution for aerospace applications. Optimization of the process parameters; the scan speed and laser power was achieved using RSM and the results were confirmed with experimental results.

II. EXPERIMENTAL PROCEDURE

A. Sample preparation

Baseplates with dimension 50 x 50 x 5 mm were sandblasted with silica grit using SBC 350 vertical sandblasting machine and wiped clean with acetone to increase the laser absorption and reduce laser reflection during deposition. Table I shows the chemical composition of the HEAs with Aluminum (Al), Cobalt (Co), Chromium (Cr), Iron (Fe), Nickel (Ni), Copper (Cu) and Titanium (Ti) powders having (99.9%) purity with an average particle size of 45 to 106 µm mixed to form AlCoCrFeNiCu (Cu-based) and AlCoCrFeNiTi (Ti-based) HEAs and supplied by F.J Brodmann & CO., L.L.C, USA. The as-received powers were used to fabricate HEA clads on an A301 steel baseplate preheated at 400 °C using a 3 kW Rofin Sinar dY044 continuous-wave laser-deposition system fitted with a KUKA robotic arm. The laser processing parameters were optimized at 1200-1600 W, a beam spot size at 2 mm, argon gas flow rate at 1.2 L/min and scan speed at 8 – 12 mm/s. Multiple tracks were produced at a 50 % overlap and angle 45 ° to the base plate.

TABLE I. Chemical composition of the Cu-based and Ti-based HEAs

Element	Al (at.%)	Co (at.%)	Cr (at.%)	Fe (at.%)	Ni (at.%)	Cu (at.%)	Ti (at.%)
Nominal	16.6	16.6	16.6	16.6	16.6	16.6	16.6
Cu-Based HEA	42.95	11.09	10.24	13.52	10.36	11.84	-
Ti-Based HEA	44.12	10.23	10.96	12.55	10.96	-	11.18

B. Microstructural analysis

The laser deposited samples were cut into sections using a Struers Discotom-2 (30800) cutting blade machine. The microstructural characterization of the sectioned HEAs samples was achieved using a Jeol-JSM-7600F Field Emission Scanning Electron Microscope fitted with an Energy Dispersive Spectroscopy.

C. Potentiodynamic polarization analysis

Potentiodynamic polarization tests were executed in a three-electrode cell consisting of a saturated silver/silver chloride electrode (Ag/AgCl) (3 m KCL) as the reference electrode, the HEAs samples as the working electrode and a graphite rod counter electrode. The samples were cleaned to remove impurities in ethanol before they were immersed in 1 mol/L NaOH solution. An Autolab Potentiostat (PGSTAT302) was used in carrying out the electrochemical measurements with Nova 1.0 software. The corrosion parameters; corrosion density (Icorr), corrosion rate (Cr), corrosion potential (Ecorr) and polarization resistance (Rp) were calculated with a Tafel extrapolation technique with a potential range between -1.5 and 2.0 V and a scan rate of 2 mV s^{-1}.

D. Response surface methodology

After using the sets of experiments to retrieve the output response; the corrosion rate (Cr), a central composite design was used to optimize and examine the influence of the laser processing parameters such as the scan speed and the laser power on the corresponding output response with a second-order polynomial equation shown below.

$$Y = \beta_0 + \sum_{i=1}^{k} \beta_i A_i + \sum_{i=1}^{k} \beta_{ii} A_i^2 + \sum_{i=1}^{k} \beta_{ij} A_i B_{ij} + \varepsilon \qquad (1)$$

Where Y is the response, A_i and B_{ij} are variables, k is the number of parameters, ε is the error, while β_i, β_{ii} and β_{ij} are interaction coefficients of the quadratic, second-order and linear terms. The data were fitted into the model and the model was validated and used to construct three-dimensional surface plots and contour plots to show the relationship between the dependent variables and the independent variables. Statistical analysis and numerical optimization were done using STAT-EASE Inc. Design-Expert Software 11, version 11.1.2.0. According to the central composite design (CCD), different runs were carried out and the final results are summarized in Table II.

TABLE II. The CCD and Experimental Parameters

High Entropy Alloys	Sample	Factor 1 A: Laser Power (P) (J/s)	Factor 2 B: Scan Speed (V) (mm/s)	Response 1: Corrosion Rate (Cr) (mm/yr) Experimental Values	Corrosion Rate (Cr) (mm/yr) Predicted Values
Cu-Based	A	1200	8	0.00231	0.0023
	B	1200	12	0.00152	0.0016
	C	1400	12	0.00187	0.0018
	D	1600	10	0.00242	0.0024
	E	1600	12	0.00203	0.0021
Ti-Based	F	1400	8	0.00211	0.0020
	G	1400	12	0.00205	0.0021
	H	1600	8	0.00322	0.0032
	I	1600	12	0.00315	0.0032

III. RESULTS AND DISCUSSIONS

A. Surface Morphology

Fig. 1 (a) and (b) show the XRD patterns of the laser-deposited AlCoCrFeNiCu and AlCoCrFeNiTi HEAs, which reveals the alloys are composed of FCC and BCC phases. According to these observations, the volume fraction of the BCC phase was more than the FCC phase attributed to the laser-deposition process [14]. The alloys had excellent metallurgical bond without defects. The Five samples of the Cu-based HEA and the four samples of the Ti-based HEA each showed dendritic microstructures.

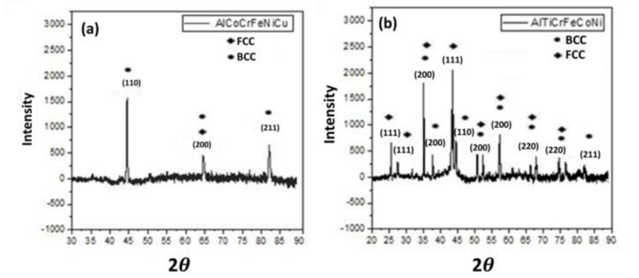

Fig.1. XRD graph of laser deposited (a) Cu-based and (b) Ti-based HEA at 1600 W and 10mm/s

B. *Potentiodynamic polarization analysis*

Polarization in electrochemistry is the potential shift away from the open current potential of a corroding system [15]. The tests in this study started at the cathodic potential to the corrosion potential, investigating the corrosion characteristics of HEAs in sodium hydroxide solution. Fig. 2 and 3 show the potentiodynamic polarization curves for the laser-deposited Ti-based and Cu-based HEAs in 1 mol/L NaOH solution respectively. Table III shows the linear fit kinetic parameters extracted from the corrosion process. In the electrochemistry principle, an increased corrosion potential, with a reduced current density, gives better corrosion resistance [16]. The higher the polarization resistance the smaller the corrosion current density and the better the corrosion resistance [17], thus, it was observed that as the corrosion current density reduces, the polarization resistance increased and as the corrosion density increases, the corrosion potential decreases with an increase in laser power from 1200 W to 1600 W. Therefore, it can be deduced that the corrosion resistance increased with an increase in laser power. The lowest corrosion density and corrosion potential were recorded at the lowest scan speed; however, as the scan speed increases, the corrosion density and potential increased with an inverse observed with the polarization resistance. A low scan speed reduces convection, which evens out the alloy's microstructure and results in fine microstructure that increases the corrosion resistance [18]. Furthermore, the corrosion resistance of the alloys can also be attributed to corrosion-resistant elements Cr, Co and Ni, which enhances the formation of passive films in alloy composition resulting in the resistance of the alloys to corrosion. Nonetheless, judging from the corrosion rates, the corrosion resistance of the alloys for Cu-based HEA can be ranked as B > C > E > A > D. Compared with the Ti-based HEA in 1 mol/L NaOH solution, the Cu-based HEA had much lower corrosion rates under the same conditions of the laser power, therefore, it can be deduced that the Cu-based HEA has better corrosion resistance in 1 mol/L NaOH solutions than the Ti-based HEA. On the other hand, the Ti-based HEA showed better polarization resistance than the Cu-based HEA attributed to the compositional difference attributed to the Ti and Al content having a large atomic radius which results in lattice distortion that helps improve the polarization resistance. Sample G of the Ti-based HEA showed the lowest corrosion rates and highest polarization resistance and judging from the results, the polarization resistance can be ranked as G > I > F > H.

TABLE III. Corrosion parameters of Cu-based and Ti-based HEAs in 1 mol/L NaOH solution

High Entropy Alloy	**Sample**	**Rp (Ωcm^{-2})**	**E_{corr} (V)**	**I_{corr} (A/cm^2)**
Cu-Based	**A**	**0.00305**	**-0.5312**	**2.243E-05**
	B	**0.00221**	**-0.6211**	**3.705E-05**
	C	**0.00200**	**-0.7413**	**4.521E-05**
	D	**0.00201**	**-0.9112**	**4.953E-05**
	E	**0.00137**	**-0.9201**	**5.26E-05**
Ti-Based	**F**	**0.00257**	**-0.6192**	**0.0873**
	G	**0.00650**	**-0.7004**	**0.00095**
	H	**0.00221**	**-0.4121**	**0.0838**
	I	**0.00609**	**-0.5144**	**0.000802**

Fig. 4 shows the surface morphology after corrosion experiments in a sodium hydroxide solution at room temperature. The surface appearance roughened losing its original smoothness with Sample A of the Cu-based HEA showing pitting at 1200 W signifying that the laser parameter played an important role as the sample suffered damage in NaOH solution at a low laser power. Qian et al. [19] reported that pitting corrosion which occurs at a low laser power may be due to microsegregation. According to Choudhuri et al. [20], micro segregation occurs when the HEA begins solidification with an FCC phase but due to alloying elements, ends up as a BCC crystal structure during solidification; this was also observed by Zollinger and Fleury [21].

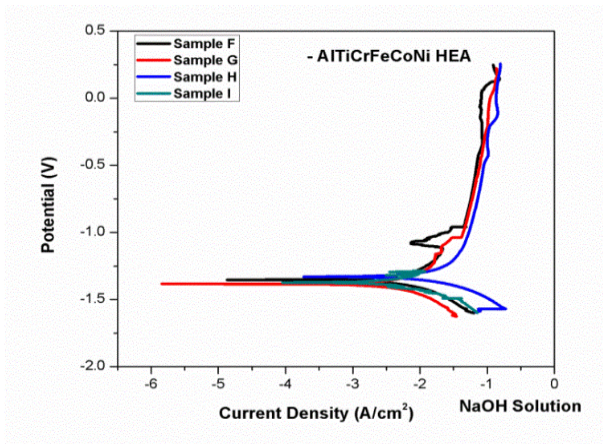

Fig.2. Tafel polarization graphs of Ti-based HEA in 1 mol/L NaOH solution at room temperature

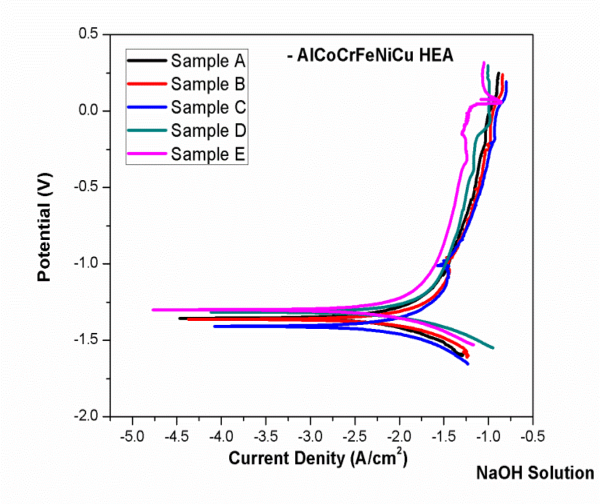

Fig.3. Tafel polarization graphs of Cu-based HEA in 1 mol/L NaOH solution at room temperature

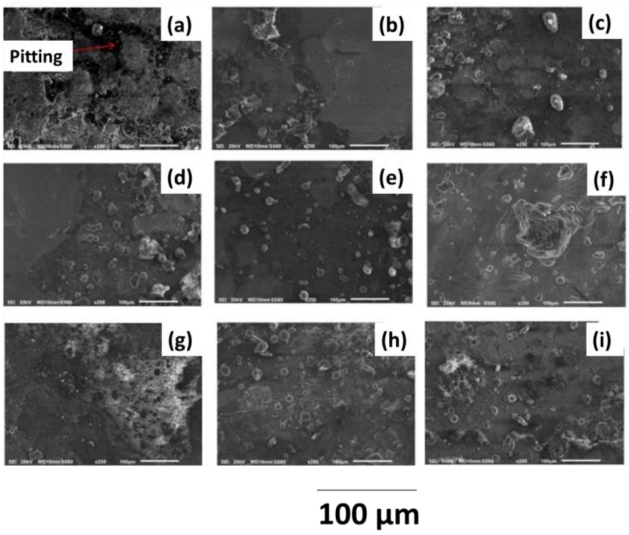

Fig.4. SEM graphs of the surface morphology after Corrosion measurements in 1 mol/L NaOH Solution (a) – (e) are Cu-based HEAs and (f) –(i) are Ti-based HEAs

C. Statistical modelling

In this study, two factors were used to optimize and evaluate the process parameters on the response such as the corrosion rate of laser-deposited HEAs in 1 mol/L NaOH solution. According to the central composite design, three to five runs are a stable variance of the predicted response is recommended [22]. The final data summarized in Table II. The CCD data were analyzed using regression linear and quadratic models with the analysis of variance results listed below.

D. Corrosion rate

The ANOVA analysis for the Cu-based and Ti-based HEA for the corrosion rate process variable is shown in Table 4. The model and the model terms are significant for the response. This is attributed to the lack-of-fit (p-values) which are less than 0.05, according to Khajeh et al. [23].
Equation 2 and 3 shows the actual factors which were used to make predictions about the output response corrosion rate for each factor.

$$\text{Corrosion rate} = +0.002312 + 1.24322E-06 * \text{Laser Power} - 0.000187 * \text{Scan Speed} \quad (2)$$

$$\text{Corrosion rate} = -0.005492 + 5.52500E-06 * \text{Laser Power} - 0.000016 * \text{Scan Speed} \quad (3)$$

TABLE IV. Regression analysis of the Response Parameter (Corrosion Rate) for the Cu-based and Ti-based HEA

High Entropy Alloy	Source	Sum of Squares	df	Mean Square	F-value	p-value	Significant Or Not
Cu-based	Model	5.100 E-07	2	2.550 E-07	82.35	0.0120	significant
	A-Laser Power	2.280 E-07	1	2.280 E-07	73.62	0.0133	significant
	B-Scan Speed	4.139 E-07	1	4.139 E-07	134.66	0.0074	significant
	Residual	6.193 E-09	2	3.097 E-09			
	Cor Total	5.162 E-07	4				
	Source	**Sum of Squares**	**df**	**Mean Square**	**F-value**	**p-value**	**Significant Or Not**
Ti-based	**Model**	1.225 E-06	2	6.126 E-07	24505.00	0.0045	**significant**
	A-Laser Power	1.221 E-06	1	1.221 E-06	48841.00	0.0029	**significant**
	B-Scan Speed	4.225 E-09	1	4.225 E-09	169.00	0.0489	**significant**
	Residual	2.500 E-11	1	2.500 E-11			
	Cor Total	1.225 E-06	3				

E. Effect of Process Variables on the Corrosion Rate

The significant relationship between the predicted and the experimental values of the output response corrosion rate for the Cu-based and Ti-based is shown in HEAs Fig. 5 (a) and (b). It was observed in both plots that the points where lined diagonally and according to Yetilmezsoy et al. [25], this indicates that the model is a good fit since this proves that there is less difference between the experimental and predicted values. The three-dimensional surface plots for the Cu-based and Ti-based HEAs used to study the interactive and individual influence of the process variables; scan speed and laser power, respectively is shown in Fig. 6 (a) and (b). The lowest corrosion rate was at 1200 W with 0.0015 mm/yr for the Cu-based HEA while the Ti-based HEA had its lowest rate at 1400 W with 0.00205 mm/yr and it was observed that the rates increased with an increase in laser power to 0.00242 for the Cu-based HEA and 0.00322 for the Ti-based HEA both at 1600 W. The numerical optimization graph used to find the optimal conditions of each factor. The results show the optimal parameters for improved corrosion rates are at laser power 1400 W and scan speed of 10 mm/s to give a corrosion rate of 0.00197 mm/yr for the Cu-based HEA and 0.002635 mm/yr for the Ti-based HEA is shown in Fig 7.

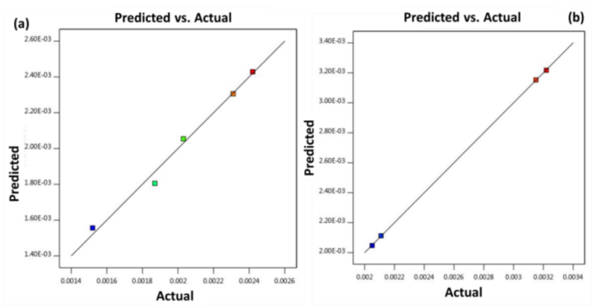

Fig.5. Parity Plots showing the Predicted and Experimental values for (a) Cu-based HEA, and (b) Ti-based HEA

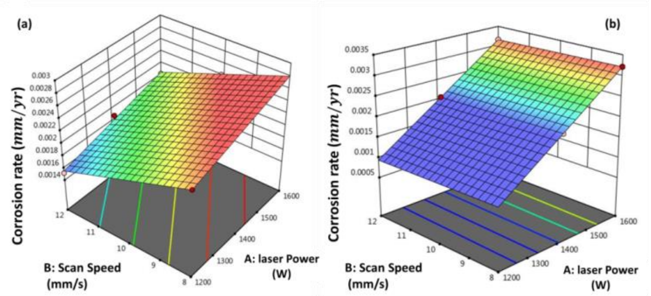

Fig.6. Showing the Surface Plots for (a) Cu-based HEA, and (b) Ti-based HEA

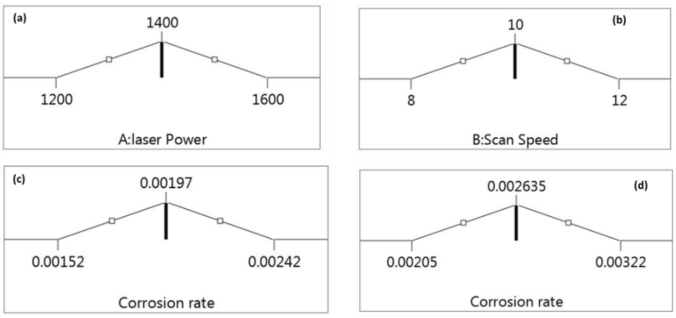

Fig.7. Numerical Optimization for (a) Cu-based HEA, and (b) Ti-based HEA

IV. Conclusion

The influence of the process variables; laser power and scan speed on the output response; corrosion rate of laser-deposited high entropy alloys in 3.5 wt. % NaOH solution was investigated using response methodology. The corrosion mechanism of both alloys was also examined at room temperature using potentiodynamic polarization, and the main results obtained are listed below:

- Both alloys showed FCC and BCC solid solution phases with dendritic structures
- The corrosion resistance increased with an increase in laser power and reduction in scan speed
- The Cu-based HEA showed better corrosion resistance, while the Ti-based HEA showed better polarization resistance attributed.
- Pitting was observed at a low laser power in the Cu-based HEA attributed to micro-segregation.
- The p-values were all lower than 0.0500 showing that all the statistical model terms were significant for the output response; corrosion rate for both alloys.
- The Cu-based HEA had a model lack of fit value of 82.35 showing that the f-value is significant and there is only a 1.20% chance that the value occurred due to noise. While the Ti-based HEA had a model F-value of 24505.00 which indicates that the value only had a 0.45% occurrence due to noise.
- The Predicted R^2 values for both alloys were in reasonable correlation with the Adjusted R^2 value, with the difference less than 0.2 each.
- The signal-to-noise ratios for both alloys were greater than 4, which is very desirable in navigating the design space.
- Optimization occurred at 1400 W laser power and a scan speed of 10 mm/s to give a corrosion rate of 0.00197 mm/yr for the Cu-based HEA and corrosion rate of 0.002635 mm/yr for the Ti-based HEA.
- Statistical modelling of the experimental results showed that the laser power is the most significant parameter with a strong influence on the corrosion rate. This validates response surface methodology as an effective tool for investigating the effect of laser parameters on the corrosion responses of laser-deposited high entropy alloys in 1 mol/L NaOH solution.

Acknowledgment

The authors will like to appreciate the Mr Samuel Skhosane of the National Laser Centre at the Council for Scientific and Industrial Research (CSIR), Mr Juwon Fayomi and Mr Uyor Uwa Orji at the Surface Engineering Research Laboratory at the Tshwane University of Technology, Pretoria, South Africa for their scientific and technical support.

References

[1] Yeh, e.a., *Nanostructured high‐entropy alloys with multiple principal elements: novel alloy design concepts and outcomes.* Advanced Engineering Materials, 2004. **6**(5): p. 299-303.

[2] Zhang, A., et al., *Rapid preparation of AlCoCrFeNi high entropy alloy by spark plasma sintering from elemental powder mixture.* Materials Letters, 2016. **181**: p. 82-85.

[3] Zhu, G., Y. Liu, and J. Ye, *Fabrication and properties of Ti (C, N)-based cermets with multi-component AlCoCrFeNi high-entropy alloys binder.* Materials Letters, 2013. **113**: p. 80-82.

[4] Ma, S. and Y. Zhang, *Effect of Nb addition on the microstructure and properties of AlCoCrFeNi high-entropy alloy.* Materials Science and Engineering: A, 2012. **532**: p. 480-486.

[5] Dong, Y., et al., *Effect of vanadium addition on the microstructure and properties of AlCoCrFeNi high*

entropy alloy. Materials & Design, 2014. **57**: p. 67-72.

[6] Chen, J., et al., *Effect of Zr content on microstructure and mechanical properties of AlCoCrFeNi high entropy alloy.* Materials & Design, 2016. **94**: p. 39-44.

[7] Nemati-Chari, R., et al., *Application of response surface methodology for study of effective strain in equal channel angular pressing of AA6061 alloy.* Proceedings of the Romanian Academy Series A-Mathematics Physics Technical Sciences Information Science, 2015. **16**(2): p. 184-192.

[8] Durakovic, B., *Design of experiments application, concepts, examples: State of the art.* Periodicals of Engineering and Natural Sciences, 2017. **5**(3).

[9] Vakili-Azghandi, M., A. Fattah-alhosseini, and M.K. Keshavarz, *Optimizing the electrolyte chemistry parameters of PEO coating on 6061 Al alloy by corrosion rate measurement: Response surface methodology.* Measurement, 2018. **124**: p. 252-259.

[10] Barcelos, A.M., et al., *Corrosion evaluation of orthodontic wires in artificial saliva solutions by using response surface methodology.* Materials Research, 2013. **16**(1): p. 50-64.

[11] Goh, K.-H., T.-T. Lim, and P.-C. Chui, *Evaluation of the effect of dosage, pH and contact time on high-dose phosphate inhibition for copper corrosion control using response surface methodology (RSM).* Corrosion Science, 2008. **50**(4): p. 918-927.

[12] Rashid, K.H. and A.A. Khadom, *Optimization of inhibitive action of sodium molybdate (VI) for corrosion of carbon steel in saline water using response surface methodology.* Korean Journal of Chemical Engineering, 2019. **36**(8): p. 1350-1359.

[13] Saeidi, M., et al., *Exploiting response surface methodology (RSM) as a novel approach for the optimization of carbon dioxide adsorption by dry sodium hydroxide.* Journal of The Chinese Chemical Society, 2018. **65**(12): p. 1465-1475.

[14] Xu, Y., et al., *Microstructure Evolution and Properties of Laser Cladding CoCrFeNiTiAlx High-Entropy Alloy Coatings.* Coatings, 2020. **10**(4): p. 373.

[15] Berradja, A., *Electrochemical Techniques for Corrosion and Tribocorrosion Monitoring: Methods for the Assessment of Corrosion Rates*, in *Corrosion Inhibitors*. 2019, IntechOpen.

[16] Wu, C., et al., *Phase evolution characteristics and corrosion behavior of FeCoCrAlCu-X0. 5 coatings on cp Cu by laser high-entropy alloying.* Optics & Laser Technology, 2017. **94**: p. 68-71.

[17] Qiu, X.-W., et al., *Microstructure and corrosion resistance of AlCrFeCuCo high entropy alloy.* Journal of alloys and compounds, 2013. **549**: p. 195-199.

[18] Yeh, J.-W., et al., *Anomalous decrease in X-ray diffraction intensities of Cu–Ni–Al–Co–Cr–Fe–Si alloy systems with multi-principal elements.* Materials chemistry and physics, 2007. **103**(1): p. 41-46.

[19] Qian, M. and J. DuPont, *Microsegregation-related pitting corrosion characteristics of AL-6XN superaustenitic stainless steel laser welds.* Corrosion science, 2010. **52**(10): p. 3548-3553.

[20] Choudhuri, D., et al., *Change in the primary solidification phase from fcc to bcc-based B2 in high entropy or complex concentrated alloys.* Scripta Materialia, 2017. **127**: p. 186-190.

[21] Zollinger, J. and E. Fleury, *Influence of Solidification Microstructure on Mechanical Properties of Al0. 8CrCuFeNi2 High Entropy Alloy.* Frontiers in Materials, 2020. **7**: p. 238.

[22] Draper, N.R. and F. Pukelsheim, *An overview of design of experiments.* Statistical Papers, 1996. **37**(1): p. 1-32.

[23] Khajeh, M., *Response surface modelling of lead pre-concentration from food samples by miniaturised homogenous liquid–liquid solvent extraction: Box–Behnken design.* Food chemistry, 2011. **129**(4): p. 1832-1838.

[24] Akossou, A. and R. Palm, *Impact of data structure on the estimators r-square and adjusted r-square in linear regression.* Int. J. Math. Comput, 2013. **20**: p. 84-93.

[25] Yetilmezsoy, K., S. Demirel, and R.J. Vanderbei, *Response surface modeling of Pb (II) removal from aqueous solution by Pistacia vera L.: Box–Behnken experimental design.* Journal of Hazardous Materials, 2009. **171**(1-3): p. 551-562.